

EXTREME CO ISOTOPIC ABUNDANCES IN THE ULIRG IRAS 13120-5453: AN EXTREMELY YOUNG STARBURST OR TOP-HEAVY INITIAL MASS FUNCTION

KAZIMIERZ SLIWA¹, CHRISTINE D. WILSON², SUSANNE AALTO³, GEORGE C. PRIVON^{4,5}

¹MPI for Astronomy, Königstuhl 17, D-69117 Heidelberg, Germany; sliwa@mpia-hd.mpg.de

²Department of Physics and Astronomy, McMaster University, Hamilton, ON L8S 4M1 Canada

³Department of Earth and Space Sciences, Chalmers University of Technology, Onsala Space Observatory, SE-439 94 Onsala, Sweden

⁴Instituto de Astrofísica, Facultad de Física, Pontificia Universidad Católica de Chile, Casilla 306, Santiago 22, Chile

⁵Departamento de Astronomía, Universidad de Concepción, Casilla 160-C, Concepción, Chile

ABSTRACT

We present ALMA ¹²CO (J=1-0, 3-2 and 6-5), ¹³CO (J=1-0) and C¹⁸O (J=1-0) observations of the local Ultra Luminous Infrared Galaxy, IRAS 13120-5453. The morphologies of the three isotopic species differ, where ¹³CO shows a hole in emission towards the center. We measure integrated brightness temperature line ratios of ¹²CO/¹³CO \geq 60 (exceeding 200) and ¹³CO/C¹⁸O \leq 1 in the central region. Assuming optical thin emission, C¹⁸O is more abundant than ¹³CO in several regions. The abundances within the central 500 pc are consistent with enrichment of the ISM via a young starburst (<7Myr), a top-heavy initial mass function or a combination of both.

Keywords: galaxies: individual(IRAS 13120-5453) — galaxies: interactions — galaxies: starburst — galaxies: abundances — submillimeter: galaxies — radiative transfer

1. INTRODUCTION

Isotopic abundances in the interstellar medium (ISM) can be used as a tracer of stellar nucleosynthesis. The ¹²C/¹³C isotope ratio is an important tracer of the relative degree of primary versus secondary processing in stars. The ¹²C atom is a primary species produced in intermediate and high-mass stars (e.g Prantzos et al. 1996). Massive stars are also responsible for the majority of ¹⁶O and ¹⁸O. The ¹³C atom is an intermediary species that is transformed into ¹⁴N. In the red giant phase of low/intermediate mass stars, ¹³C is lifted to the envelope via convection (Wilson & Matteucci 1992) and eventually released into the ISM. Massive stars are short-lived and will start to enrich the ISM in ¹²C in $\sim 10^6$ years while ¹³C enrichment needs $\sim 10^9$ years (e.g. Vigroux et al. 1976).

Ultra/Luminous Infrared Galaxies (U/LIRGs) are extreme starbursts offering great laboratories to study high-mass star formation. It has long been observed that ¹³CO emission is unusually weak relative to ¹²CO (~ 20 -40; Aalto et al. 1991; Casoli et al. 1992) compared to that from normal disk galaxies (~ 10 ; e.g. Paglione et al. 2001). Pioneering work by Casoli et al. (1992) and Henkel & Mauersberger (1993) presented several scenarios to explain this unusual emission ratio such as optical depth effects, abundance variations via some mechanism such as photo-dissociation, inflowing low metallicity gas or enrichment of the ISM and a two-phase molecular

medium consisting of a diffuse envelope where ¹²CO can better self-shield than ¹³CO. Recent radiative transfer modeling of the molecular gas in several U/LIRGs is consistent with high [¹²CO]/[¹³CO]¹ abundance ratios (>90; Sliwa et al. 2013, 2014; Henkel et al. 2014; Papadopoulos et al. 2014; Tunard et al. 2015).

Recent work on the [¹⁶O]/[¹⁸O] abundance in U/LIRGs using *Herschel* H₂O and OH observations have shown varying values from ≤ 30 for Mrk231 González-Alfonso et al. (2010), around 50-150 for Arp220 (González-Alfonso et al. 2014) and Zw 049.057 (Falstad et al. 2015) and ≥ 500 for Arp 299 (Falstad et al. 2017) and NGC 4418 (González-Alfonso et al. 2014). König et al. (2016) used Atacama Large Millimeter/submillimeter Array (ALMA) CO data to show that the [¹⁶O]/[¹⁸O] ≥ 900 for NGC 1614. The high [¹⁶O]/[¹⁸O] abundance ratios are believed to be due to inflowing gas and the low values to stellar processing.

IRAS 13120-5453 (dubbed the “Yo-Yo”) is a nearby ULIRG ($D_L = 144$ Mpc) with a far-infrared luminosity ($L_{\text{FIR}} = 1.5 \times 10^{12} L_{\odot}$; Sanders et al. 2003) similar to that of Arp 220. The system has been classified as a post-merger (Haan et al. 2011). X-ray emission is consistent with a Compton-thick active galac-

¹ Square brackets denote an abundance ratio while all other ratios are integrated brightness temperature ratios

tic nucleus (AGN; Iwasawa et al. 2011) and contributes $\sim 18\%$ to the infrared luminosity (Sturm et al. 2011). The *Herschel* Fourier Transform Spectrometer (FTS) observed multiple high- J CO lines as well as CI, H₂O, NII, OH and more (Rosenberg et al. 2015; Mashian et al. 2015; Pearson et al. 2016; Privon et al. 2017). Privon et al. (2017) shows that the HCN/HCO⁺ line ratio observed with ALMA suggests an increased HCN abundance via turbulent heating.

In this Letter, we present new ALMA Cycle 2 observations of IRAS 13120-5453 where we have detected three ¹²CO transitions, ¹³CO and C¹⁸O $J=1-0$. The morphology of the three species differs and offers insight into the mechanism that may be controlling the [¹²CO]/[¹³CO] ratio. We show that massive stars have enriched the ISM in ¹²C and ¹⁸O and drive the observed line ratios in IRAS 13120-5453.

2. OBSERVATIONS AND LINE RATIOS

ALMA was used to observe IRAS 13120-5453 in Cycle 2 using Bands 3, 7 and 9 (Table 1). We calibrated all datasets manually in CASA v4.5.3 (McMullin et al. 2007) using standard calibration steps. We implemented two iterations of phase-only self calibration on the ¹²CO datasets, which did not significantly alter the morphology of IRAS 13120-5453. We CLEAN the datacubes using a Briggs robust weighting of 0.5 down to 1σ level with channels widths of 20 or 35 km s⁻¹. Integrated intensity maps were created using the CPROPs (Rosolowsky & Leroy 2006) masking routine² and only channels that contained masked emission were included down to 1.5σ . All maps were primary beam corrected (Figure 1).

Table 1. Observational Data

Parameter ^a	¹² CO $J=1-0$	¹² CO $J=3-2$	¹² CO $J=6-5$	¹³ CO $J=1-0$	C ¹⁸ O $J=1-0$
Obs Data	2015 July 03	2015 June 07	2015 June 09	2015 July 22	2015 July 22
Calibrators	J1107-4449	J1427-4206	J1256-0547	J1107-4449	J1107-4449
	J1551-1755	Titan	J1427-421	J1427-421	J1427-421
	Titan	J1329-5608	J1329-5608	J1329-5608	J1329-5608
	J1329-5608	J1315-5334	J1427-4206		
Integration Time (s)	652	867	1567	3117	3117
Median PWV (mm)	2.4	0.63	0.37	3.2	3.2
Median T _{sys} (K)	64	135	984	82	82
Flux ^b (Jy km s ⁻¹)	126 (±2) [± 13]	1265 (± 15) [± 130]	2460 (± 25) [± 370]	2.21 (±0.05) [±0.2]	2.1 (±0.05) [±0.2]
rms (mJy beam ⁻¹)	1.5 (20 km s ⁻¹)	1.1 (20 km s ⁻¹)	16 (20 km s ⁻¹)	0.3 (35 km s ⁻¹)	0.3 (35 km s ⁻¹)
Resolution (arcsec)	0.58 × 0.35	0.39 × 0.29	0.25 × 0.16	0.55 × 0.41	0.55 × 0.41

^aOther line present in the data will be discussed in forthcoming paper (Sliwa et al in prep.)

^bUncertainties in curved and square brackets denote measurement and calibration uncertainties, respectively.

All three ¹²CO transitions have similar morphologies with a single nucleus.

The ¹³CO $J=1-0$ emission is more interesting with no emission above 1.5σ near the central nucleus ($\sim 0.85'' \times 0.3'' = 590 \text{ pc} \times 210 \text{ pc}$) and two relatively strong emission regions outside the nucleus. The region lacking emission is within the starburst region (0.5 kpc) measured by Privon et al. (2017). *Interestingly, the C¹⁸O emission is relatively strong where there is no ¹³CO emission. In the central 0.3'' spectrum (Figure 2), it is evident that C¹⁸O is stronger than ¹³CO.* We note that

C¹⁸O may be partially contaminated by HNCO ($5_{0,5} - 4_{0,4}$) and several higher-energy transitions that lie on top of the C¹⁸O line. Along a line of sight, the maximum contamination is likely 30% determined from the peak of the HNCO ($5_{0,5} - 4_{0,4}$) transition; however, we do not make any corrections since this is an upper limit to the contamination and may only contribute to part of the C¹⁸O line profile.

Selective UV photodissociation of the rare CO isotopologues should affect both ¹³CO and C¹⁸O, with the nominally rarer C¹⁸O affected the most. Thus it could not produce the observed relative line intensity ratio variations between them, let alone boost the C¹⁸O abundance to be higher than ¹³CO in the inner 500 pc of IRAS 13120-5453. If optical depth effects were causing the ring, C¹⁸O should also be observed in a ring since

² The routine finds pixels greater than 3σ in 2 channels and then includes emission down to some σ level around the pixel. This method is excellent at excluding spurious noise pixels

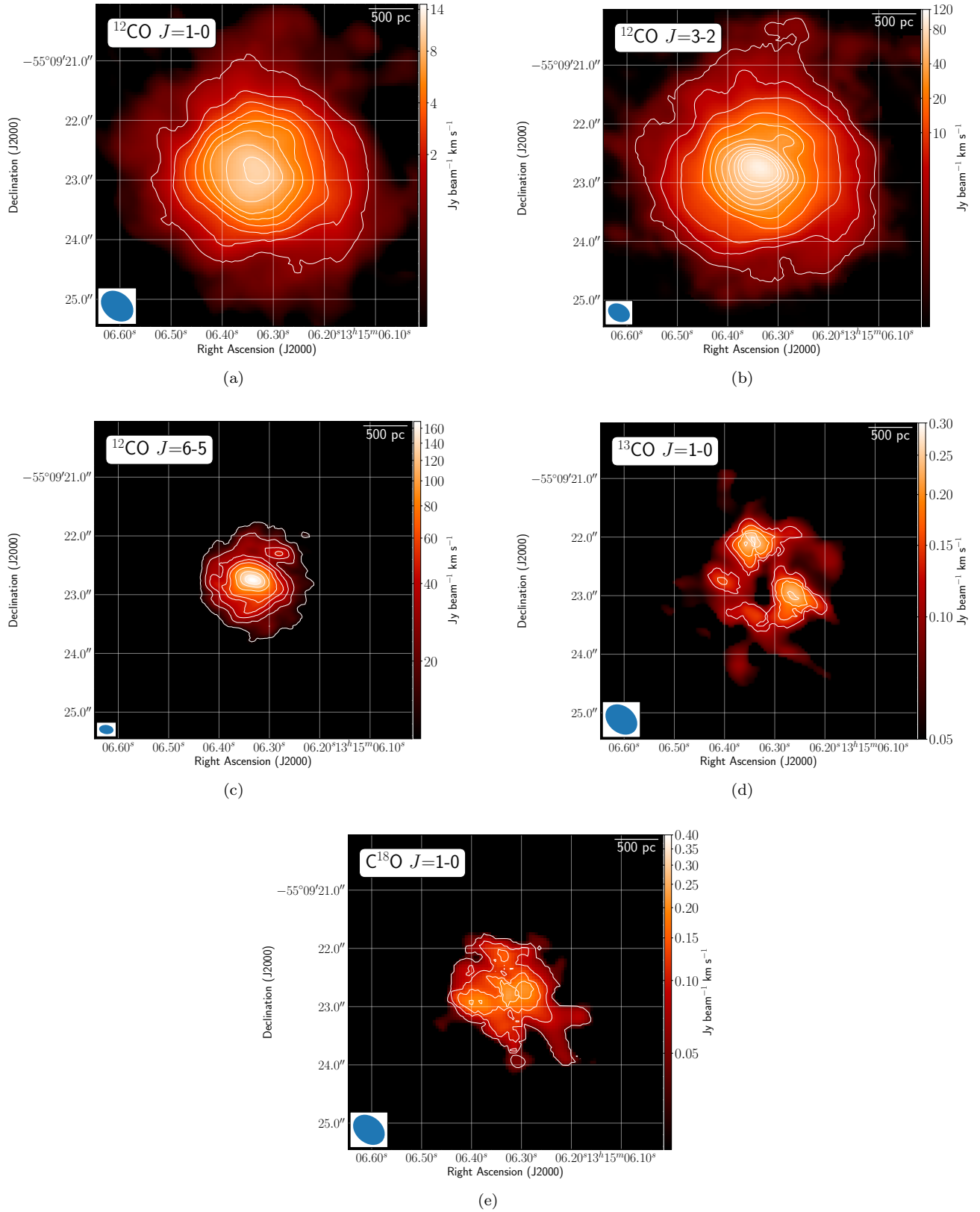


Figure 1. Integrated intensity maps for IRAS 13120-5453: (a) $^{12}\text{CO } J=1-0$, (b) $^{12}\text{CO } J=3-2$, (c) $^{12}\text{CO } J=6-5$, (d) $^{13}\text{CO } J=1-0$ and (e) $\text{C}^{18}\text{O } J=1-0$. Ellipse in the bottom left corner represents the synthesized beam.

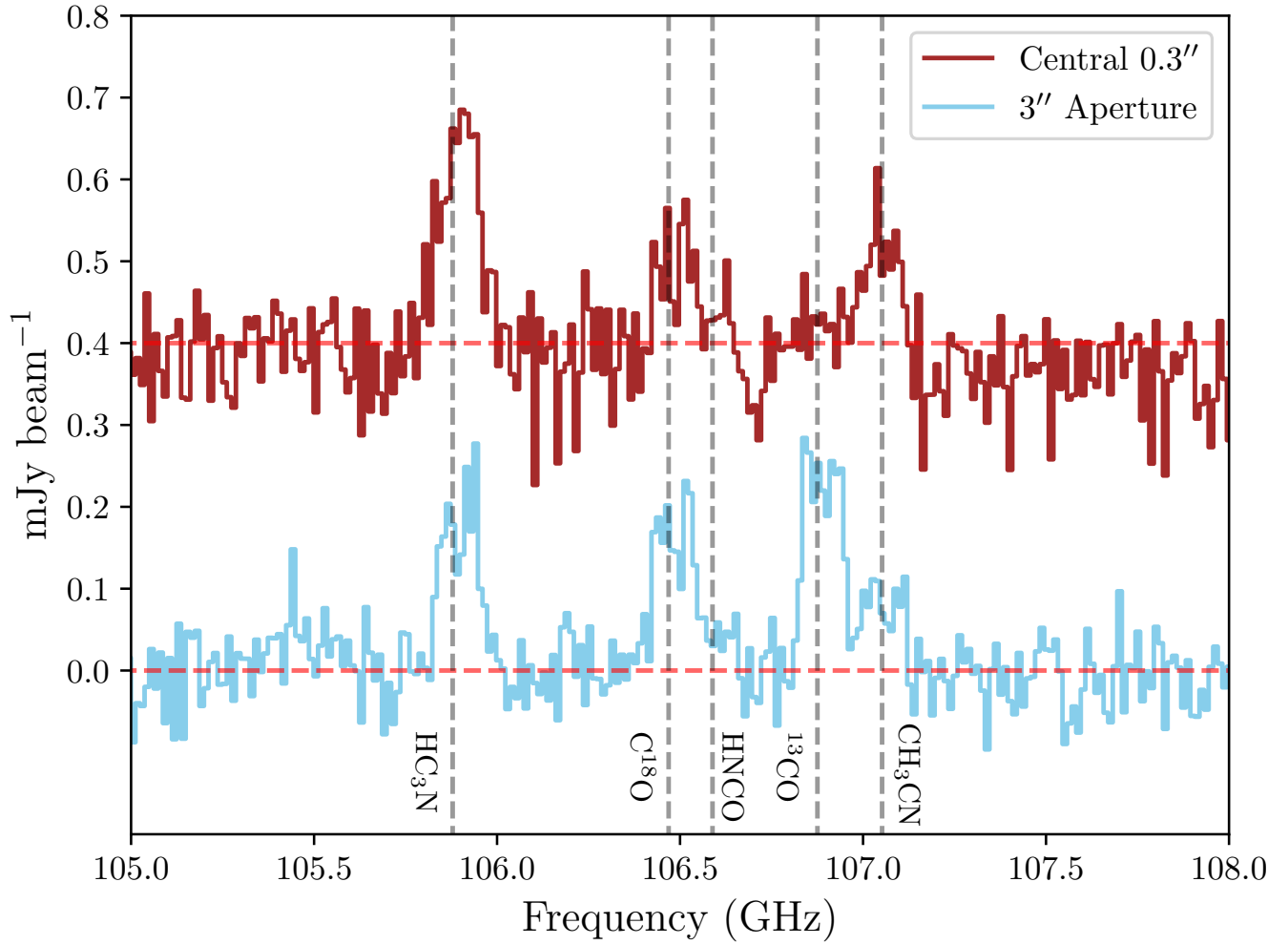


Figure 2. Averaged spectra for (top) the central 0.3'' diameter aperture scaled down by a factor of 6 and shifted up by 0.4 mJy beam⁻¹ and (bottom) over a 3'' diameter aperture. Identified spectral lines are marked with vertical dashed lines ($z=0.03112$). For HNCO, we mark the $5_{0,5}-4_{0,4}$ transition.

both ^{13}CO and C^{18}O are assumed to be optically thin. The Band 3 observations, observed 19 days apart, have similar uv -coverage adding confidence to the observed differences in morphology and corresponding intensities between the lines. The three ^{12}CO maps (Figure 1) also show that as we go to higher-resolution ($J=1-0 \rightarrow J=6-5$) we do not see a ring in ^{12}CO .

Integrated brightness temperature ($I = \int T_B dV$) line ratio maps can offer some insight into the conditions of the molecular gas. We create the following line ratios maps:

$$R_{10} = \frac{I^{12\text{CO}(1-0)}}{I^{13\text{CO}(1-0)}}$$

$$Y_{10} = \frac{I^{13\text{CO}(1-0)}}{I^{\text{C}^{18}\text{O}(1-0)}}$$

$$Z_{10} = \frac{I^{12\text{CO}(1-0)}}{I^{\text{C}^{18}\text{O}(1-0)}}$$

We match the ^{12}CO , ^{13}CO and C^{18}O $J=1-0$ maps to an angular resolution of $0.60'' \times 0.45''$. We then create line ratio maps by cutting emission below 2σ in each map and converting the units from $\text{Jy beam}^{-1} \text{ km s}^{-1}$ to $\text{K}(T_B) \text{ km s}^{-1}$ (Figure 3).

The R_{10} line ratio shows a wide range of values from ~ 10 to over 250. While values of around 30 are common for local U/LIRGs (e.g. Sliwa et al. 2012, 2013, 2014), values exceeding 100 have never been observed before in local ULIRGs. The Y_{10} line ratio ranges from 0.2 to over 4. Values below 1 are rare in extragalactic systems where normal disk galaxies have an average Y_{10} value of ~ 6 and normal starbursts show Y_{10} values of ~ 3 (Jiménez-Donaire et al. 2017). Arp 220 (Greve et al. 2009; Matsushita et al. 2009) and the high- z ULIRG SMM J2135-0102 (Danielson et al. 2013) show a Y_{10} ratio of 1 while the LIRG merger remnant, NGC 2623, shows a Y_{10} ratio of ~ 1.8 (Sliwa et al. in preparation). The Z_{10} values range from ~ 20 -140 and are similar to those of Mrk 231 (González-Alfonso et al. 2010), Arp 220 (González-Alfonso et al. 2014) and Zw 049.057 (Falstad et al. 2015).

3. EXTREME ISOTOPIIC ABUNDANCES

We argue that IRAS 13120-5453 has an extreme isotopic abundance ratio when compared to normal star-forming galaxies. The brightness temperature line ratio of species A and B can be expressed as

$$R = \frac{I^A}{I^B} = \frac{T_{\text{ex}}^A (1 - e^{-\tau_A})}{T_{\text{ex}}^B (1 - e^{-\tau_B})} \quad (1)$$

where T_{ex} is the excitation temperature and τ is the optical depth of the particular species and transition. For simplicity, we assume local thermal equilibrium (LTE; i.e. $T_{\text{ex}}^A = T_{\text{ex}}^B = T_{\text{kin}}$). (Significant radiative trapping for the abundant species can give $T_{\text{ex}}^A = T_{\text{kin}}$ while $T_{\text{ex}}^B < T_{\text{kin}}$.) If species B is optically thin and species A is

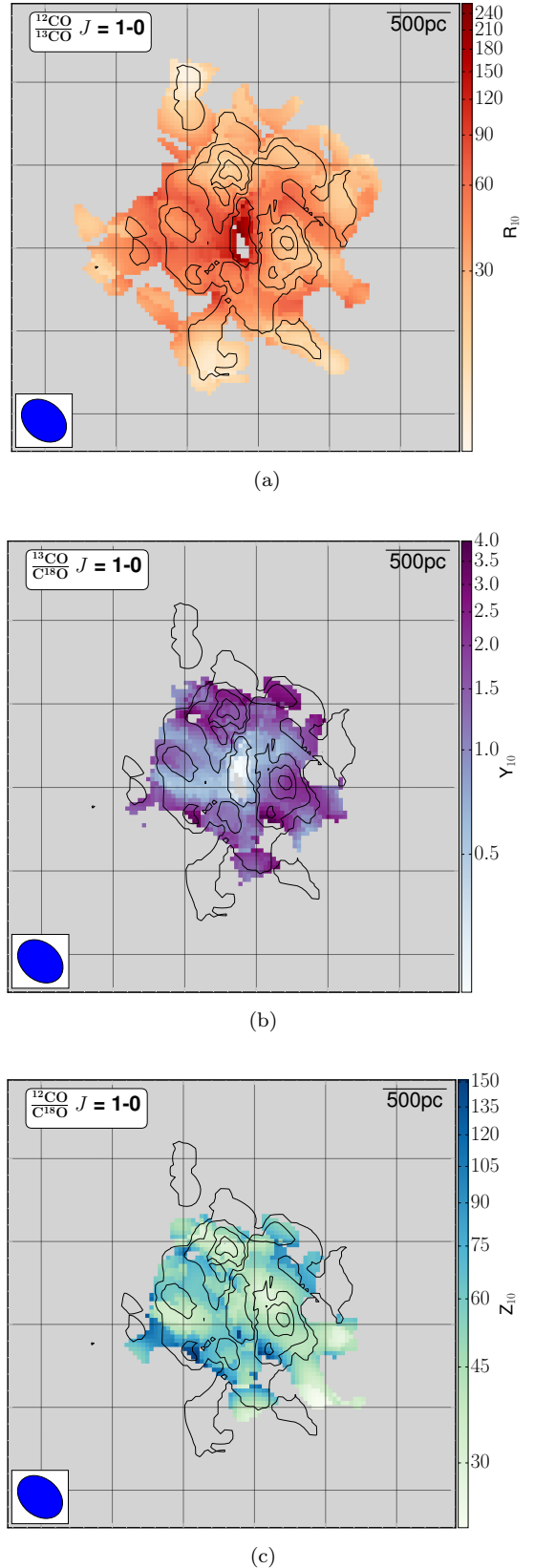


Figure 3. Line brightness temperature ratio maps for (a) R_{10} , (b) Y_{10} and (c) Z_{10} . Each map has an angular resolution of $0.6'' \times 0.45''$. Black contours are of ^{13}CO $J=1-0$ added as a guide.

optically thick, then

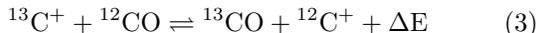
$$R \sim \frac{1}{\tau_B} \sim \frac{[A]}{[B]} \frac{1}{\tau_A}. \quad (2)$$

If ^{12}CO is optically thick, the line ratios R_{10} and Z_{10} are lower limits to the relative abundance of ^{12}CO to ^{13}CO and C^{18}O since the observed line ratio is attenuated by the optical depth of ^{12}CO . Since R_{10} and $Z_{10} \gg 1$, both ^{13}CO and C^{18}O must be optically thin. Thus the Y_{10} line ratio of < 1 implies that *C^{18}O is more abundant than ^{13}CO in the central region*; this would still be true even if the HNC/O contamination were to reach 50%.

4. ROOT OF THE EXTREME ABUNDANCES

Photo-dissociation: Since C^{18}O is bright relative to ^{13}CO , we can rule out selective photo-dissociation as the dominant mechanism since both C^{18}O and ^{13}CO would be destroyed by UV radiation.

Fractionation: The most important carbon isotope exchange is



(Watson et al. 1976) where the forward reaction dominates in cold environments (< 30 K) favouring the formation of ^{13}CO . In hot environments, both directions have equal probability (Roueff et al. 2015). We use the non-LTE code RADEX (van der Tak et al. 2007) and a Bayesian likelihood code (Kamenetzky et al. 2012) to constrain the molecular gas physical conditions within the ~ 400 pc central region using only the ^{12}CO observations. We fit the ^{12}CO $J=1-0$ line with a Gaussian profile of $\text{FWHM}=375$ km s $^{-1}$. The most probable solution is warm, dense molecular gas with a $T_{\text{kin}} = 130_{-77}^{+400}$ K, $\log(n_{\text{H}_2}) = 4.2_{-0.0}^{+2.4}$ cm $^{-3}$ and $\log(M(\text{H}_2)/M_{\odot}) = 7.8_{-0.1}^{+1.0}$. Since the molecular gas is not cold enough for the forward reaction to dominate, we can rule out fractionation as a possible mechanism affecting the abundance. We also note that C^{18}O does not undergo fractionation and should reflect stellar processing (Langer et al. 1984).

Infalling Gas: The merger process can drive a gas inflow towards the nuclear regions (e.g. Hopkins et al. 2006; Kewley et al. 2006; Ellison et al. 2008). The Galaxy has an increasing radial gradient in the $^{12}\text{CO}/^{13}\text{CO}$ abundance ratio ranging from 30 in the center to >100 at large radii (e.g. Milam et al. 2005). Jiménez-Donaire et al. (2017) have shown that a trend with $^{13}\text{CO}/\text{C}^{18}\text{O}$ exists in disk galaxies as well with an average value of 6.0 ± 0.9 . Analyses of close galaxy pairs have shown that their metallicities are lower than similar field galaxies (Kewley et al. 2006; Ellison et al. 2008). Rupke et al. (2008) found that the dilution of the nuclear metallicity (Z) due to gas inflow is $Z_{\text{final}}/Z_{\text{initial}} \sim 0.5$; therefore, if we assume an initial $^{12}\text{CO}/^{13}\text{CO}$ ratio of 30, we would expect a final ratio of ~ 60 . This

would not be sufficient to explain the observed line ratios in the central regions, particularly the brighter C^{18}O emission.

Nucleosynthesis: Enrichment of the ISM via massive stars is a likely mechanism. Massive stars are the dominant sources of ^{12}C , ^{16}O and ^{18}O while ^{13}C is predominately released from low/intermediate mass stars. Simulations show that the metallicity in the merger increases when the star-formation rate increases significantly, especially near the end of the merger process (Torrey et al. 2012).

For nucleosynthesis enrichment to be plausible, the starburst must be young. With a normal initial mass function (IMF) such as the Kroupa IMF (e.g. Kroupa 2001) within ~ 6 Myr, all stars $>30M_{\odot}$ will have gone supernova ejecting material. Using the nucleosynthesis yield calculations for core-collapse supernovae (CC-SNe) of Nomoto et al. (2006) and assuming a total star-forming molecular mass of $10^9 M_{\odot}$ and an initial metallicity of $Z=0.02$ ($\sim Z_{\odot}$), the $^{12}\text{CO}/^{13}\text{CO}$ value of the ejected material after 6Myr will be ~ 575 , while after 7Myr when all stars above $25M_{\odot}$ will have gone supernova, the $^{12}\text{CO}/^{13}\text{CO}$ will be ~ 60 .

If the starburst is older (>7 Myr), an alternative solution is a top-heavy IMF. Bartko et al. (2010) find a top-heavy IMF for the Galactic center of $dN/dm \propto m^{-0.45 \pm 0.3}$. Habbergham et al. (2010) also invoke a top-heavy IMF to explain the excess of CCSNe in interacting/mergers galaxies when compared to isolated galaxies. Assuming only stars of $10-130M_{\odot}$ will eject material vis CCSNe, a Kroupa IMF will produce a $^{12}\text{CO}/^{13}\text{CO}$ abundance of 40 while a flat, top-heavy IMF ($\phi_m \propto m^0$) will produce a $^{12}\text{CO}/^{13}\text{CO}$ abundance of 270. While a flat IMF is an arbitrary choice, a top-heavy IMF of some variety is required if the starburst is older than ~ 6 Myr to explain our observed abundances in the central region. We also note that a combination of both a young-starburst and a top-heavy IMF is also plausible. Future work into the star formation history of IRAS 13120-5453 is required to clarify the starburst-age/IMF degeneracy.

We thank the referee for improving this manuscript. This paper uses the following ALMA data: ADS/JAO.ALMA#2012.1.00306.S + ADS/JAO.ALMA#2013.1.00379.S. ALMA is a partnership of ESO (representing its member states), NSF (USA) and NINS (Japan), together with NRC (Canada) and NSC and ASIAA (Taiwan) and KASI (Republic of Korea), in cooperation with the Republic of Chile. The JAO is operated by ESO, AUI/NRAO and NAOJ. The NRAO is a facility of the NSF operated under cooperative agreement by Associated Universities, Inc.

G.C.P. was supported by a FONDECYT Postdoctoral Fellowship (No. 3150361).

Facility: ALMA

REFERENCES

- Aalto, S., Johansson, L. E. B., Booth, R. S., & Black, J. H. 1991, *A&A*, 249, 323
- Bartko, H., Martins, F., Trippe, S., et al. 2010, *ApJ*, 708, 834
- Casoli, F., Dupraz, C., & Combes, F. 1992, *A&A*, 264, 55
- Danielson, A. L. R., Swinbank, A. M., Smail, I., et al. 2013, *MNRAS*, 436, 2793
- Ellison, S. L., Patton, D. R., Simard, L., & McConnachie, A. W. 2008, *AJ*, 135, 1877
- Falstad, N., González-Alfonso, E., Aalto, S., & Fischer, J. 2017, *A&A*, 597, A105
- Falstad, N., González-Alfonso, E., Aalto, S., et al. 2015, *A&A*, 580, A52
- González-Alfonso, E., Fischer, J., Isaak, K., et al. 2010, *A&A*, 518, L43
- González-Alfonso, E., Fischer, J., Graciá-Carpio, J., et al. 2014, *A&A*, 561, A27
- Greve, T. R., Papadopoulos, P. P., Gao, Y., & Radford, S. J. E. 2009, *ApJ*, 692, 1432
- Haan, S., Surace, J. A., Armus, L., et al. 2011, *AJ*, 141, 100
- Habergham, S. M., Anderson, J. P., & James, P. A. 2010, *ApJ*, 717, 342
- Henkel, C., & Mauersberger, R. 1993, *A&A*, 274, 730
- Henkel, C., Asiri, H., Ao, Y., et al. 2014, *A&A*, 565, A3
- Hopkins, P. F., Hernquist, L., Cox, T. J., et al. 2006, *ApJS*, 163, 1
- Iwasawa, K., Sanders, D. B., Teng, S. H., et al. 2011, *A&A*, 529, A106
- Jiménez-Donaire, M. J., Cormier, D., Bigiel, F., et al. 2017, *ApJL*, 836, L29
- Kamenetzky, J., Glenn, J., Rangwala, N., et al. 2012, *ApJ*, 753, 70
- Kewley, L. J., Geller, M. J., & Barton, E. J. 2006, *AJ*, 131, 2004
- König, S., Aalto, S., Müller, S., et al. 2016, *A&A*, 594, A70
- Kroupa, P. 2001, *MNRAS*, 322, 231
- Langer, W. D., Graedel, T. E., Frerking, M. A., & Armentrout, P. B. 1984, *ApJ*, 277, 581
- Mashian, N., Sturm, E., Sternberg, A., et al. 2015, *ApJ*, 802, 81
- Matsushita, S., Iono, D., Petitpas, G. R., et al. 2009, *ApJ*, 693, 56
- McMullin, J. P., Waters, B., Schiebel, D., Young, W., & Golap, K. 2007, in *Astronomical Society of the Pacific Conference Series*, Vol. 376, *Astronomical Data Analysis Software and Systems XVI*, ed. R. A. Shaw, F. Hill, & D. J. Bell, 127
- Milam, S. N., Savage, C., Brewster, M. A., Ziurys, L. M., & Wyckoff, S. 2005, *ApJ*, 634, 1126
- Nomoto, K., Tominaga, N., Umeda, H., Kobayashi, C., & Maeda, K. 2006, *Nuclear Physics A*, 777, 424
- Paglione, T. A. D., Wall, W. F., Young, J. S., et al. 2001, *ApJS*, 135, 183
- Papadopoulos, P. P., Zhang, Z.-Y., Xilouris, E. M., et al. 2014, *ApJ*, 788, 153
- Pearson, C., Rigopoulou, D., Hurley, P., et al. 2016, *ApJS*, 227, 9
- Prantzos, N., Aubert, O., & Audouze, J. 1996, *A&A*, 309, 760
- Privon, G. C., Aalto, S., Falstad, N., et al. 2017, *ApJ*, 835, 213
- Rosenberg, M. J. F., van der Werf, P. P., Aalto, S., et al. 2015, *ApJ*, 801, 72
- Rosolowsky, E., & Leroy, A. 2006, *PASP*, 118, 590
- Roueff, E., Loison, J. C., & Hickson, K. M. 2015, *A&A*, 576, A99
- Rupke, D. S. N., Veilleux, S., & Baker, A. J. 2008, *ApJ*, 674, 172
- Salpeter, E. E. 1955, *ApJ*, 121, 161
- Sanders, D. B., Mazzarella, J. M., Kim, D.-C., Surace, J. A., & Soifer, B. T. 2003, *AJ*, 126, 1607
- Sliwa, K., Wilson, C. D., Iono, D., Peck, A., & Matsushita, S. 2014, *ApJL*, 796, L15
- Sliwa, K., Wilson, C. D., Petitpas, G. R., et al. 2012, *ApJ*, 753, 46
- Sliwa, K., Wilson, C. D., Krips, M., et al. 2013, *ApJ*, 777, 126
- Sturm, E., González-Alfonso, E., Veilleux, S., et al. 2011, *ApJL*, 733, L16
- Torrey, P., Cox, T. J., Kewley, L., & Hernquist, L. 2012, *ApJ*, 746, 108
- Tunnard, R., Greve, T. R., Garcia-Burillo, S., et al. 2015, *ApJ*, 815, 114
- van der Tak, F. F. S., Black, J. H., Schöier, F. L., Jansen, D. J., & van Dishoeck, E. F. 2007, *A&A*, 468, 627
- Vigroux, L., Audouze, J., & Lequeux, J. 1976, *A&A*, 52, 1
- Watson, W. D., Anicich, V. G., & Huntress, Jr., W. T. 1976, *ApJL*, 205, L165
- Wilson, T. L., & Matteucci, F. 1992, *A&A Rv*, 4, 1
- Zhang, Z.-Y., Gao, Y., Henkel, C., et al. 2014, *ApJL*, 784, L31